Catal Lett (2016) 146:1397–1407
DOI 10.1007/s10562-016-1764-z

Promotion Effects of Cesium on Perovskite Oxides for Catalytic Soot Combustion

Wen Shao[1] · Zhongpeng Wang[1] · Xiaomin Zhang[1] · Liguo Wang[1] · Zhenmin Ma[1] · Qian Li[1] · Zhaoliang Zhang[1]

Received: 29 April 2016 / Accepted: 9 May 2016 / Published online: 18 May 2016

Abstract The cesium-promoted $LaCoO_3$ perovskite-type catalysts were synthesized for catalytic soot combustion. The cesium promoter was introduced into the perovskite system via two different ways with the same Cs loading: one is Cs doping ($La_{0.8}Cs_{0.2}CoO_3$), and the other is Cs supporting ($Cs/LaCoO_3$). The physicochemical properties of the catalysts were characterized by XRD, N_2-sorption, SEM, EDS, H_2-TPR, NO oxidation and NO_x sorption techniques. For Cs-supported sample, the promotion effect on the redox properties of transition metal has been observed. The catalytic NO oxidation activity on Cs-supported sample was higher than that on Cs-doped sample due to the improved reducibility. Under O_2 atmospheres, the two kinds of Cs-containing catalysts exhibited similar ignition activities under tight conditions with soot ignition temperature decreased to about 350 °C, which can be related to the enhanced oxygen mobility and the improved contact between soot and catalysts. In the presence of NO_x, the superior soot oxidation activity on Cs-supported catalyst was related to its higher NO_2 productivity, larger NO_2 consumption and more stored nitrates accessible in soot oxidation process. Thus, the different ways to introduce cesium have different impacts on the properties and activities of the perovskite catalysts.

Graphical Abstract Cesium surface promotion is much more effective than the bulk promotion in soot oxidation over $LaCoO_3$ perovskite catalysts.

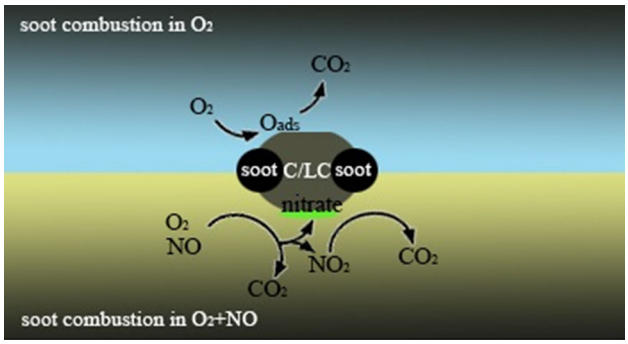

Keywords Perovskite · Catalytic activity · Soot combustion · NO oxidation

1 Introduction

Diesel engine has higher fuel-efficiency than petrol engine due to its high compression ratio. Thus, diesel exhaust differs from petrol engine exhaust in two major characteristics. Firstly, diesel exhaust contains a far higher amount of particulate matter, and NO_x. Secondly, the exhaust is far leaner, that is, far less unburned hydrocarbon and carbon monoxide than a typical exhaust from petrol engines [1, 2]. The single soot particles of few nanometers present an amorphous core surrounded by a graphitic shell. Several adverse effects on health have been attributed to soot particles. A fraction of these particles (the so-called PM-10, with size smaller than 10 μm) can penetrate the respiratory tract and are deposited on lungs increasing cancer risk, asthma and bronchitis [3]. And the NO_x emissions have multi-fold hazard for the atmosphere, environment and human health, due to the formation of fine

✉ Zhongpeng Wang
chm_wangzp@ujn.edu.cn

✉ Liguo Wang
chm_wanglg@ujn.edu.cn

[1] School of Resources and Environment, University of Jinan, 106 Jiwei Road, Jinan 250022, People's Republic of China

particles, ozone smog, acid rain and eutrophication [4, 5]. Nowadays, the focus of the reduction of harmful diesel emissions is mainly on particulate matter and NO_x.

For soot abatement, particles can be trapped with acceptable efficiency from diesel exhaust gas by means of filtration. Diesel particulate filter (DPF), an efficient way to trap soot, helps to meet the stringent limits. The question is particulates spontaneously burn in air at about 600–625 °C, while this temperature range is not regularly achieved in the typical diesel vehicle operations for sufficient periods of time to enable self-regeneration [6]. The DPF needs to be regenerated when backpressure reaches alarm value. The conventional strategy for DPF regeneration is electrical heating, yet it is energy-consuming. A more economic route, continuous regeneration through coating catalysts, was developed to simplify the post-process system. The performance of DPF regeneration largely depends on the catalysts activity; hence it is urgent to find a stable and active catalyst compatible with this route [7, 8].

For NO_x abatement in diesel exhaust, selective catalytic reduction of NO_x (SCR) and NO_x storage/reduction (NSR) technology are widely accepted as the commercialized strategies. In terms of NSR, which is also called as lean NO_x trap (LNT), NO_x reduction is achieved by selectively storing NO_x under lean conditions, and then nonselectively reducing the stored NO_x under short, rich (reducing) excursions [9, 10]. SCR has a high NO_x purification rate but has been essentially developed for heavy-duty trucks and buses due to deficiencies in the infrastructure with respect to urea supply [11]. Besides, NO_x exhaust emissions can also be removed via simultaneous NO_x-soot removal. Considering the pollutants emitted from diesel engines as a whole, the most feasible removal method is the integration of NO_x traps and oxidation catalysts [12].

To accomplish the regeneration of DPF at lower temperatures, various catalysts, such as noble metals [13], transition metals [14, 15], perovskites [16], spinels [17], earth alkali metals [18] and alkali metals [19], have been developed to decrease soot ignition temperature. Therein, the ABO_3-type perovskite, where A is a rare-earths (La, Ce, Pr) and alkaline earths (Cs, Sr, Ba, Ca) larger ($r_A \sim 0.90$ Å) than B transition metals (Co, Fe, Cu, Ni, Mn, Cr, Al) ($r_B \sim 0.51$ Å) [20] have attracted increasing interest for diesel soot combustion in view of its excellent catalytic activity. The oxidation capability of perovskites mainly depends on the B-site cations which can be changed by partially substituting A and/or B with suitable metals [5, 20]. Thus the capability of $LaCoO_3$ in soot removal has been studied [7, 21, 22], and two traditional strategies were reported to promote the activity of $LaCoO_3$ catalysts. One is to replace cations at one or both of the A and B sites. This method leads to the generation of oxygen vacancies or the variation of valence state of metal ions at both sites. The other is preparation into macroporous morphology which can significantly improve the contact conditions between soot and catalyst. Special attention [23–25] has also been paid to alkali metals-containing perovskite catalysts. In the case of catalytic soot oxidation, the first role of alkali is to increase the contact between soot particles and catalyst surface since this parameter is known as a critical step in soot oxidation reaction. Other beneficial effects of alkali were ascribed to the formation of nitrate-nitrite surface species in the presence of NO_x which participate in the soot combustion process [26, 27]. Cesium is a representative type alkali metal which provided strong alkalinity. It has been found that the substitution of alkali metal ions into A site enhanced the activity by the order: Cs > K > Na [28, 29]. The previous studies, however, mainly focus on A-site substitution by alkali metals [30, 31]; alkali metals supported on perovskites have received little attention. In fact, the different ways to introduce cesium have different impacts on the properties and activities of these catalysts. In order to investigate the promotion effect of Cs on $LaCoO_3$ perovskite oxides for catalytic soot combustion, Cs-doped perovskite ($La_{0.8}Cs_{0.2}CoO_3$) and Cs-supported perovskite ($Cs/LaCoO_3$) are prepared and characterized, since they possess a good thermal stability and catalytic activity for soot combustion.

2 Experimental

2.1 Catalyst Preparation

Perovskite catalysts were synthesized by a citric sol–gel method as follows: The reagents (nitrate salts of desired oxides) first dissolved in distilled water in stoichiometric amounts. A given amount of citric acid dissolved in deionized water is added in above solution as a ligand, the molar ratio of citric acid to the total metal ions is 1:1. The solution is stirring in water bath at 80 °C for 7 h. The sample slowly becomes sol, and then gel. In the next, the wet gel was dried in air flow at 120 °C overnight to obtain a dried precursor. Pre-calcination at 350 °C for 2 h to make nitrate decompose, the corresponding mixed oxides were further calcined at 800 °C for 4 h in air flow to form spongy powder of final catalysts.

For the supported catalyst $Cs/LaCoO_3$, the $LaCoO_3$ perovskite was firstly prepared as above; then an aqueous solution containing a desired amount of $CsNO_3$ was impregnated on $LaCoO_3$ with stirring. After drying at 120 °C for 12 h, the catalyst was calcined at 800 °C for 4 h in air flow. The cesium loading in $LaCoO_3$ is about 10 wt% which is in line with that of $La_{0.8}Cs_{0.2}CoO_3$ sample. For convenience, the as-prepared catalysts of $LaCoO_3$,

$La_{0.8}Cs_{0.2}CoO_3$, and $Cs/LaCoO_3$ are denoted as LC, LCC, C/LC, respectively.

2.2 Catalyst Characterization

XRD was conducted with a BRUKER-AXS D8Adance X-ray Diffractometer using Cu Kα radiation, at 40 kv and 40 mA, in the scanning angle (2θ) range of 20°–80° at a scanning speed of 6° min^{-1}. The JCPDS database (International Centre for Diffraction Data, 1996.) was used for the phase identification.

The textural properties of the mixed oxides samples were analyzed by N_2 adsorption/desorption isotherms which were performed using a Micromeritics ASAP 2020 surface area analyzer after outgassing at 300 °C for 5 h prior to analysis. The specific surface areas were calculated with the Brunauer–Emmett–Teller (BET) equation, and the pore volume was derived with the Barrett–Joyner–Halenda (BJH) method on the basis of the adsorption data.

The morphology of the catalysts was determined with a QUANTA FEG250 scanning electron microscope (SEM). And energy dispersive spectroscopy (EDS) were obtained on an Oxford X-MAX-50 system.

Temperature-programmed reduction with H_2 (H_2-TPR) experiments were performed in a quartz reactor with a thermal conductivity detector (TCD) to monitor the H_2 consumed. Catalysts were pretreated in situ at 500 °C for 50 min in a flow of N_2 (50 ml/min). After cooled down to room temperature, TPR was conducted at 10 °C/min up to 900 °C in a 50 ml/min flow of 5 vol% H_2 in Ar.

2.3 Catalyzed NO Oxidation into NO_2

NO oxidation on the catalysts was investigated by a temperature-programmed oxidation (TPO) technique in the same experimental apparatus as used in NO_x storage experiments. The catalysts were pretreated in situ at 500 °C for 1 h in He. After cooled down to room temperature, a feed gas containing 1000 ppm NO + 5 vol% O_2 in He was introduced and NO_x oxidation was started at a heating rate of 4 °C/min until 700 °C. Concentrations of NO, NO_2 and NO_x from the reactor outlet were monitored by a chemiluminescence NO_x analyzer.

2.4 NO_x Adsorption and Desorption Experiments

The NO_x storage performance was studied by isothermal adsorption of NO_x followed by temperature programmed desorption (TPD) of adsorbed species. The catalysts were finely ground, sized in 40–80 mesh for NO_x adsorption–desorption experiments. The TPD experiments were carried out in a quartz flow reactor (i.d. = 6 mm and L = 240 mm). Catalyst was pretreated in situ at 500 °C for 1 h in He and then cooled to 300 °C. When the temperature had stabilized at 300 °C, the flow gas was switched to 1000 ppm NO and 5 vol% O_2 in He at a rate of 100 ml/min for 1.5 h for thermal NO_x adsorption. When adsorption finished as the monitor figure stabilized, He was switched to sweep and reactor cooled down to 100 °C. After there was no NO_x any more, TPD started at a heating rate of 10 °C/min until 700 °C. Concentration of NO, NO_2 and NO_x from the reactor outlet were monitored by a chemiluminescence NO_x analyzer.

2.5 Catalytic Activity Testing

The catalytic reactions for soot combustion were performed by a temperature-programmed oxidation technique (TPO) in a fixed-bed flow reactor. A model soot of Printex-U from Degussa was mixed with the catalyst in a weight ratio of 1:9 in an agate mortar with a pestle for 10 min to obtain a tight contact between soot and catalyst, while with a spatula for 2 min to achieve loose contact. A 50 mg sample of the soot/catalyst mixture was pretreated in a flow of He (100 ml/min) at 200 °C for 0.5 h to remove surface-adsorbed species. After cooling down to room temperature, a gas flow with 5 vol% O_2 in He or 1000 ppm NO + 5 vol% O_2 in He (50 ml/min) was introduced and then TPO was started at a heating rate of 4 °C/min until 700 °C. NO_x (NO and NO_2) and CO_x (CO and CO_2) in the effluent were online analyzed by the chemiluminescence NO_x analyzer (Model 42i-HL, Thermo Electron Corporation) and a gas chromatograph (GC) (SP-6890, Shandong Lunan Ruihong Chemical Instrument Corporation, China), respectively. The characteristic temperatures from the TPO profiles, T_5 and T_{50} are defined as the temperatures at which 5 and 50 % of soot is converted, respectively. The selectivity to CO_2 formation (S_{CO_2}) is defined as the percentage CO_2 outlet concentrations. NO_x removal is evaluated by maximum NO_x removal rate (C_m) during the TPO process.

In addition, the N_2 formation during TPO reactions was analyzed using a TCD gas chromatograph (Shimazu GC-8A) with columns of Porapak Q for separating CO_2 and N_2O and molecular sieve 5A for N_2 and O_2.

3 Results and Discussion

3.1 XRD Analysis

XRD patterns of the catalysts are displayed in Fig. 1. It can be seen that all the catalysts display typical diffraction peaks of $LaCoO_3$ perovskite (JPCDS 48-0123), demonstrating that the perovskite structures are well maintained

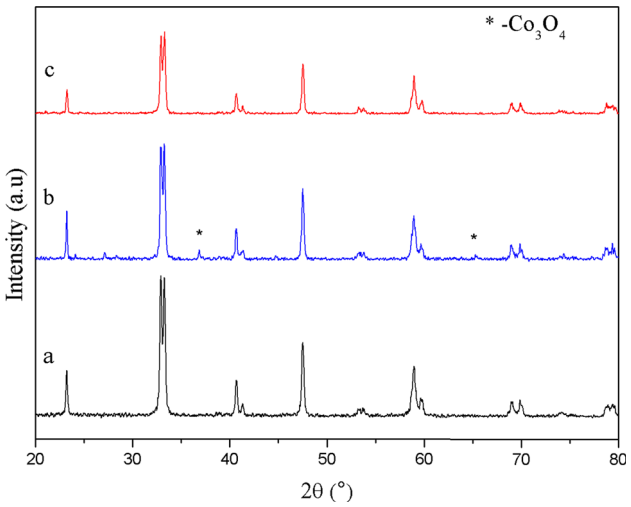

Fig. 1 X-ray diffraction patterns of **a** LC, **b** LCC, **c** C/LC

after the partial substitution of Lanthanum by Cesium or the direct impregnation of Cesium. Meanwhile, several weak diffraction peaks of Co_3O_4 had been found in LCC sample. The segregation of trace amounts of Co_3O_4 in the present study may be due to the high calcinations temperature up to 800 °C [32]. However, there are no obvious peak position shifts after Cs introduced. Only a tiny difference in the lattice constant a_c is found among the catalysts (LC: 5.44539 ± 0.0029, LCC: 5.44288 ± 0.0030, C/LC: 5.44379 ± 0.0054). For the both Cs-containing samples, no diffraction signals related to Cs species are detected, suggesting the high dispersion or small crystallites size of Cs species. The evolution of crystallites size determined by the Debye–Scherrer equation tends to decrease in the presence of cesium (LC: 54.7 nm, LCC: 43.1 nm, C/LC: 42.5 nm).

3.2 Textural Characteristics

The textural properties of the mixed oxides obtained by nitrogen adsorption at −196 °C, are summarized in Table 1. The specific surface area reaching 5.2 $m^2\ g^{-1}$ for the LC sample, decreased upon introduction of the cesium metal cations. Such a reduction in the surface area may be related to the aggregation of the metallic oxides blocking the smaller pores and/or causing some structural rearrangements.

Applying the BJH method to the isotherm desorption branch, average pore size of 13–15 nm is assigned to the mixed oxides, and thus, gas molecule diffusion in these pores is not the rate-determining step for adsorption and desorption [33].

3.3 SEM and EDS

Figure 2 shows the SEM and EDS images of different samples, exhibiting that introduction of Cs^+ has an evident effect on the morphology and structure of samples. Figure 2a showed the $LaCoO_3$ perovskite-type oxides had a spherical shape. As seen in Fig. 2b, c, the particle size of the samples after doped or supported by cesium became larger and their particle tend to cohere. Obviously, the size distribution of the Cs-containing samples is more irregular. Moreover, the particle size of C/LC sample seemed larger than that of the LCC sample. Some fine grains adhering to the sample were observed on C/LC in Fig. 2c, and high surface Cs content was showed by EDS. Meantime, less surface oxygen on C/LC was observed than that on LCC and LC in EDS. It is noted that the particle size measured here with SEM are far bigger than the average crystallite size calculated from XRD analysis, implying the accumulation of crystallites in the sample.

Table 1 Textual properties and NO_x storage capacity of the oxide catalysts

Samples	S^a_{BET} ($m^2\ g^{-1}$)	V^b_p ($cm^3\ g^{-1}$)	D^c_p (nm)	NAC[d] (μmol g^{-1})	NSC[e] (mg g^{-1})	BT[f] (s)	Consumed H_2[g] (μmol g^{-1})
LC	5	0.017	13.3	317.6	0.22	48	1973.7
LCC	1	0.005	12.0	455.9	0.63	108	616.6
C/LC	1	0.005	15.8	356.1	0.74	83	3176.8

[a] BET surface area

[b] Total pore volume

[c] Average pore size

[d] NO_x adsorption capacity

[e] NO_x storage capacity at temperature range 300–450 °C

[f] Breakthrough time: the time to reach an outlet NO_x concentration equal to 10 % of inlet NO_x concentration

[g] H_2 uptake at the range 200–500 °C in H_2-TPR tests

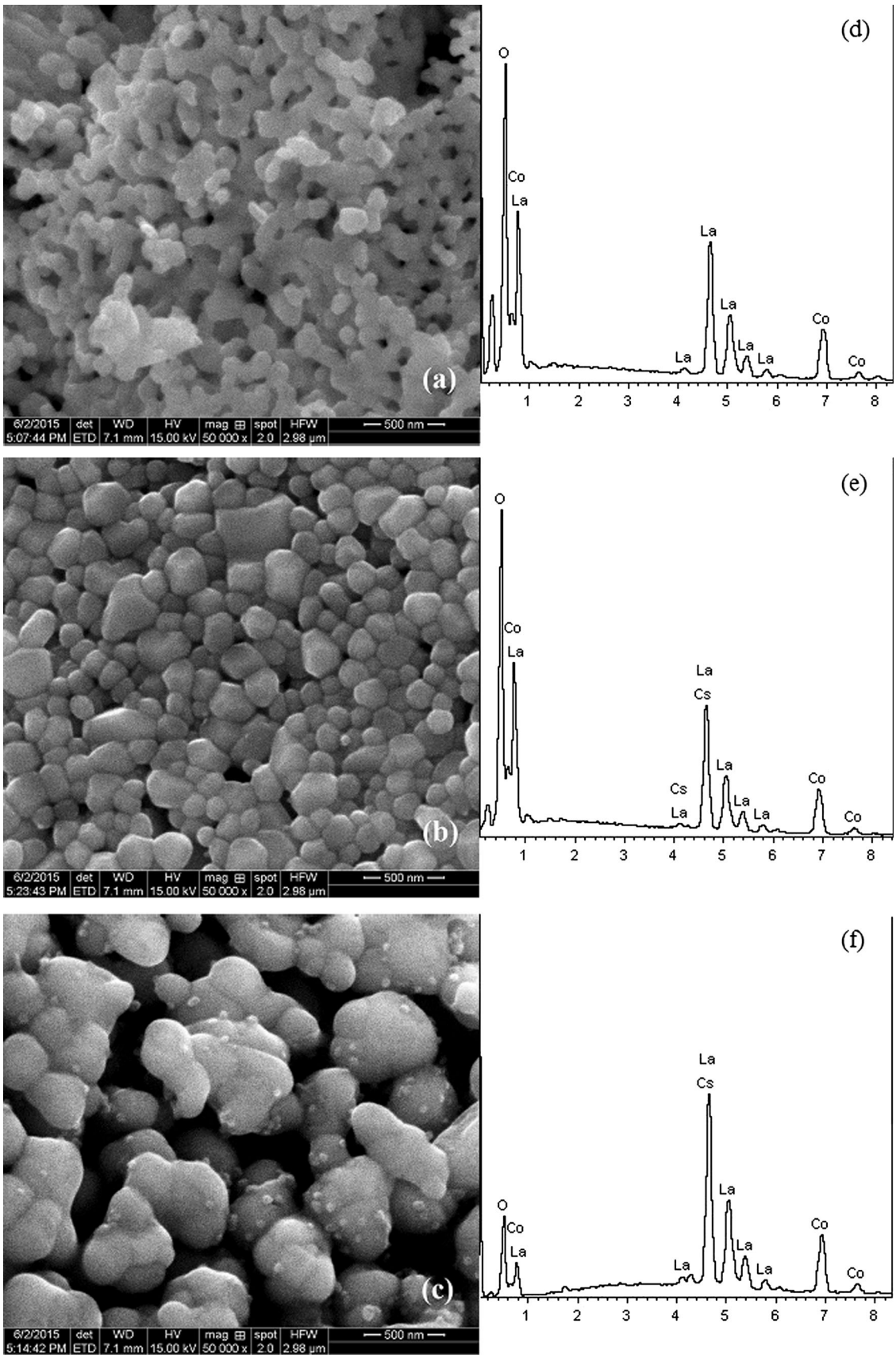

Fig. 2 SEM photographs and EDS spectra of the catalysts: **a**, **d** for LC, **b**, **e** for LCC, **c**, **f** for C/LC

3.4 H_2-TPR

The redox properties of the catalysts were characterized by H_2-TPR presented in Fig. 3. It can be seen from the ignition temperature in H_2 consumption that the reducibility was decreased after Cs introduced. The LC and LCC samples show similar reduction profiles containing two main peaks, which correspond to the stepwise reduction of $LaCoO_3$ perovskite. The reduction peak at lower temperature (300–450 °C) is attributed to the removal of non-stoichiometric excess O accommodated within the lattice and the reduction of Co^{3+} to Co^{2+}, forming oxygen-deficient perovskite (La_2CoO_4); the higher reduction peak (500–650 °C) is assigned to the further reduction of La_2CoO_4 to Co^0 [7, 34–37]. As for Cs-doped sample, the reduction peaks were shifted to higher temperatures range, indicating decreased reducibility of LCC. The broadened and asymmetric shapes for C/LC imply that there exists more than one stage for the reduction of trivalent cobalt to metallic cobalt. The hydrogen uptake was assigned to two consecutive reduction steps i.e., Co^{3+} to Co^{2+} and Co. The low temperature peak becomes larger for C/LC indicating that surface Cs introduction promotes Co^{3+} reduction to Co^{2+}, in comparison with LC and LCC. And it was implied that the Co^{3+} played more important role than Co^{2+} in the CB catalytic oxidation [38].

As indicated in the following TPO reactions, the reducible oxygen species on the catalyst surface in temperature range 200–500 °C can be accessible in the soot oxidation process. The consumed H_2 in this range are summarized in Table 1. The higher H_2 consumption, i.e., the larger amount of oxygen species can be found on C/LC sample than that on LC and LCC samples, which may facilitate soot oxidation.

3.5 NO Oxidation

NO_2 is considered as an important intermediate in both NO_x storage and soot oxidation. NO_x storage materials are generally more effective in adsorbing NO_2 than NO, and $LaCoO_3$ catalyst was reported to be highly active for NO oxidation [39]. The NO-to-NO_2 conversions for the LC, LCC and C/LC catalysts are plotted as a function of temperature in Fig. 4. Conversion increased with increasing temperature within the kinetically limited regime and achieved a maximum as the equilibrium limit was reached. It should be noted that in the absence of catalyst <3 % of NO is oxidized to NO_2 because of the effect of temperature [40].

As can be seen from Fig. 4, NO can be readily oxidized to NO_2 on all catalysts even at low temperature with about 13 % of NO converted. When the temperature exceed 300 °C, the oxidation of NO was accelerated on the LC and C/LC catalysts with a maximum NO_2 level at 400 °C. Interestingly, the maximum NO conversion on LCC was shifted to high temperature together with a weak shoulder peak at 350 °C. From the maximum NO_2 level in the TPO profiles, the NO_2 production capacity decreases by the following order: LC > C/LC > LCC. These results clearly indicate that the presence of Cs permits to hider NO_2 formation which is consistent with previous research [41]. The decreased NO_2 formation may be due to the decreased reducibility and surface area after Cs introduced. In addition, we noticed a decrease in outlet concentration of NO_x at low temperature on Cs-contained samples and can be explained by the NO_x storage capacity of alkali-containing system [26, 27].

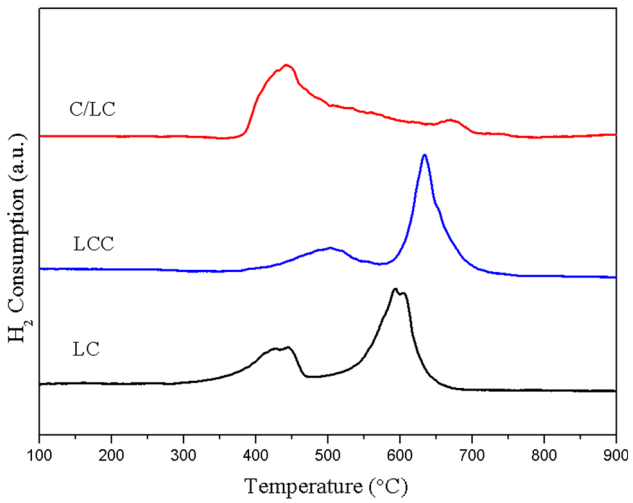

Fig. 3 H_2-TPR patterns of mixed oxides samples

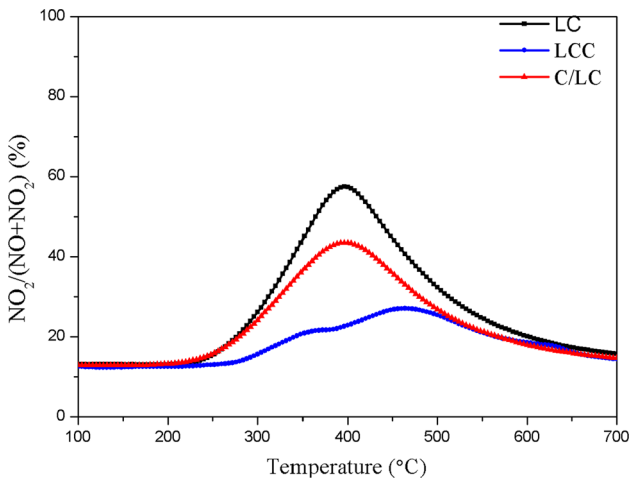

Fig. 4 Catalyzed NO oxidation to NO_2 over the oxides samples

3.6 NO_x Absorption and Desorption Experiments

The adsorption profiles of NO_x of the samples at 300 °C are presented in Fig. 5. In the initial stage, as almost no NO_x was detected in the outlet stream. The breakthrough time (the time to reach an outlet NO_x concentration equal to 10 % of inlet NO_x concentration) was largely increased after alkali metal introduced, which may be related to the improved basic properties. The NO_x adsorption capacity (NAC) was also improved in the presence of Cs for the same reasons. However, considering that the NO_2 production capacity was decreased, the enhanced basicity may predominate during the NO_x adsorption process. Indeed, redox sites are necessary to oxidize NO to NO_2 and basic sites are necessary to store NO_2 in the form of nitrates [42]. The most common NO_x adsorption mechanism was proposed that the storage process was accomplished via two parallel routes: one was the nitrate route, and the other was nitrite route [43, 44]. The nitrate route is through the oxidation of NO to NO_2 on the catalyst surface, and its subsequent adsorption to form nitrates, while nitrite route is interpreted by the stepwise oxidation of NO in the presence of oxygen to form nitrite ad-species, which were progressively oxidized to nitrates. Generally speaking, the amounts of adsorbed NO_x species follow the order: $NO_2 > NO + O_2 \gg NO$ [45]. That is, nitrate species were mainly detected upon adsorption of NO_2.

Figure 6 presents desorption profiles of NO_x from the oxides catalysts after NO_x adsorption at 300 °C, in which NO is the predominant species, with almost no NO_2. The NO_x storage capacity (NSC) of the oxide catalysts calculated from the desorption curve at temperature range 300–450 °C are listed in Table 1. The desorption peaks of three catalysts are at temperature range higher than 300 °C which mainly belong to nitrate decomposition [46]. As seen in Fig. 6, there is only one desorption peak at 320 °C for LC sample. While for Cs-contained samples, the NO_x desorption follows a two-step process, a shoulder peak at low temperature (300–450 °C) and another desorption peak

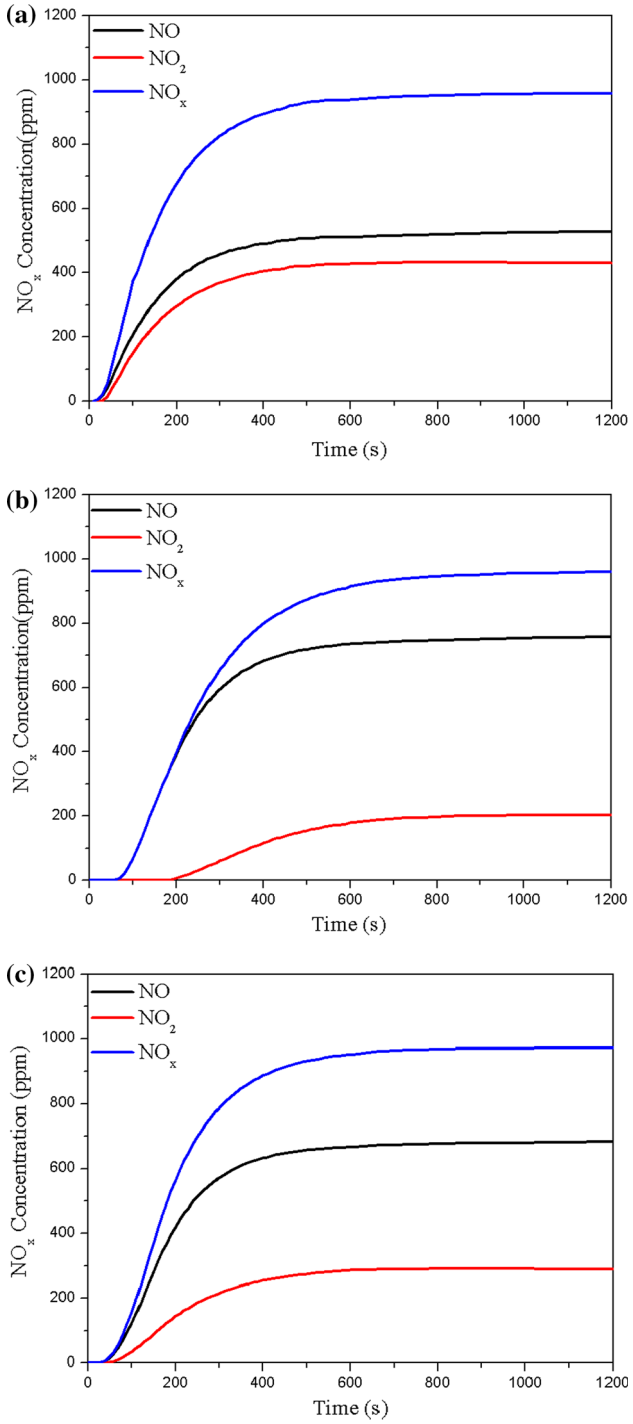

Fig. 5 NO_x adsorption on **a** LC, **b** LCC and **c** C/LC catalysts at 300 °C

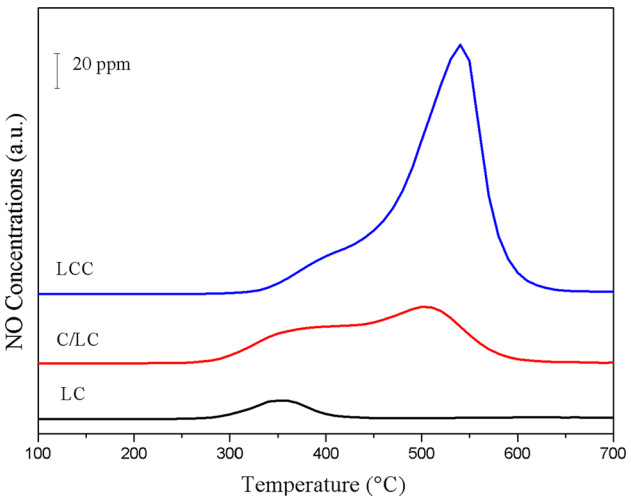

Fig. 6 NO_x desorption from the catalysts with adsorption temperature at 300 °C

at high temperature range. The desorption peak at higher temperature may be ascribed to Cs related nitrates. The stability of the formed nitrates and the temperature of NO_x release are related to the basicity of the cations [27]. Obviously, the introduction of cesium promoted the NO_x storage capacity of $LaCoO_3$, and it's more facile to form surface nitrate species for LCC than C/LC.

3.7 Soot Oxidation with O_2 and NO + O_2

The soot conversion profiles obtained during catalytic tests under tight conditions with O_2 and NO + O_2 are plotted as a function of temperature in Fig. 7. The derived parameters of T_5, T_{50}, ΔT_{50}, S_{CO_2} and C_m are summarized in Table 2.

Under O_2 atmosphere, the blank experiment shown in Fig. 7a was performed mixing the soot with SiO_2, and the ignition temperature was 470 °C which is in agreement with our previous work [11]. The ignition activity was improved moderately after Cs introduced with T_5 shifted from 359 °C for LC to about 350 °C. The oxidation activity of perovskites has been ascribed to their ionic conductivity, their oxygen sorption properties, to oxygen mobility within their lattice, and their reducibility [20]. When a perovskite is heated at high temperature, oxygen vacancies can be formed. The oxygen vacancies favour the catalytic activity in oxidation reaction because they increase the lattice oxygen mobility [47, 48]. In the present study, the promotion effect of oxygen mobility within perovskite lattice was interpreted as the interaction between Cs and Co (La), which might weaken the Co (La)-O band, thus facilitating the mobility of the oxygen species, and leading to higher concentration of surface oxygen species. The active surface oxygen species are transported through the surface oxide layer to the catalyst-soot interface, where the soot particles are oxidized to carbon oxides. On the other hand, the electropositive nature of alkali and alkali earth metal oxides could result in a strengthening of carbon–oxygen bonds and a corresponding weakening of carbon–carbon bonds by electron transfer to the carbon substrate. In addition, it has also been widely accepted that the cesium can increase the exchange surface between soot particles and the catalyst surface due to the low melting point of alkali metals which may decrease ignition temperature. Interestingly, the parameter T_{50} of C/LC is higher than two other samples. The decreased T_{50} activity may be related to the surface alkali oxides covering partly the oxygen vacancies.

It can be seen from Fig. 7b and Table 2 that the presence of NO positively affects the activity of all the oxides catalysts over the entire soot conversion range. In comparison with the non-catalyzed soot oxidation, soot

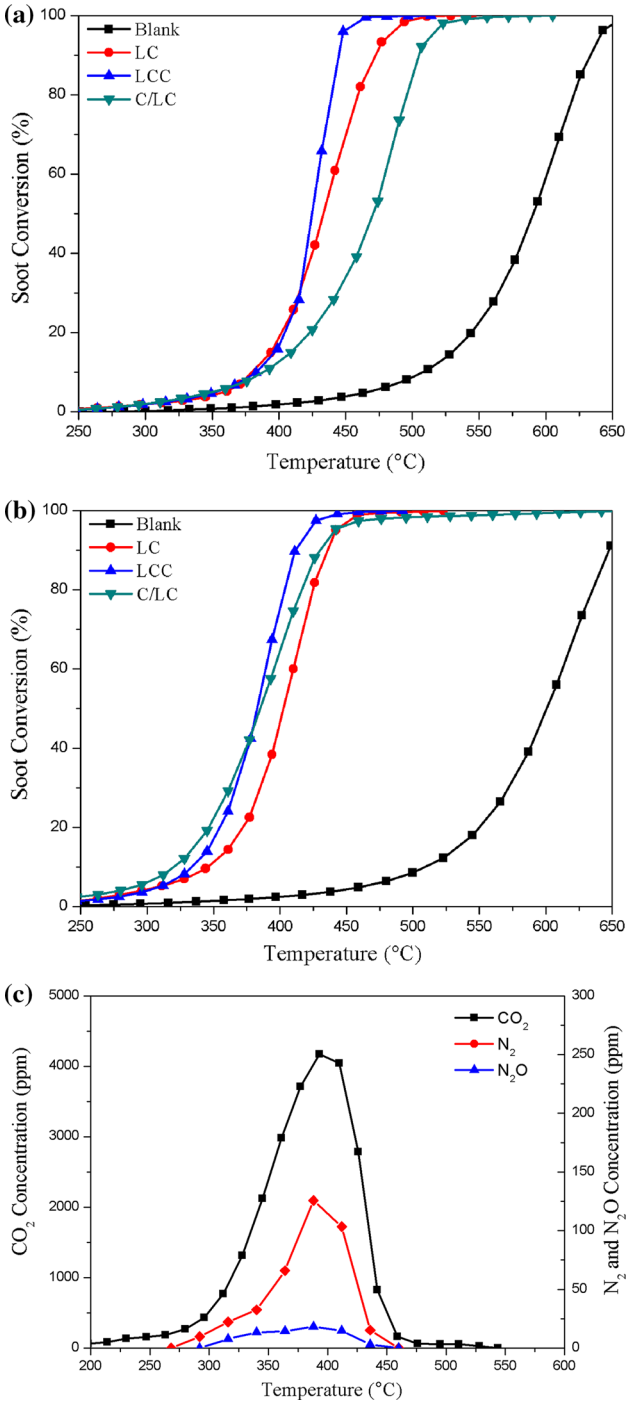

Fig. 7 Catalytic oxidation of soot over perovskite-derived mixed oxides in O_2 (**a**), NO + O_2 (**b**) and temperature-programmed reaction of the simultaneous NO_x-soot removal over the C/LC catalyst (**c**)

conversion curves over the mixed oxides shift to lower temperature range with T_5 and T_{50} decreased. The catalytic activity seems obviously promoted by the reaction between NO_x and soot. Based on our previous research [42], the reaction scheme responsible for the high catalytic

Table 2 Catalytic performance for soot combustion under tight conditions with O_2 and $NO + O_2$

Samples	O_2			$NO + O_2$				ΔT_{50} (°C)
	T_5 (°C)	T_{50} (°C)	S_{CO_2} (%)	T_5 (°C)	T_{50} (°C)	S_{CO_2} (%)	C_m (%)	
Blank	470	590	37.8	461	601	49.1	9.4	−11
LC	359	434	99.8	307	402	98.8	9.6	32
LCC	351	425	97.1	306	383	97.2	32.4	42
C/LC	350	471	96.7	288	385	94.6	29.1	86

performance in catalytic combustion of soot particles in the presence of NO_x was proposed as follows [Eqs. (1)–(3)]:

$$2NO + O_2 \rightarrow 2NO_2 \quad (1)$$

$$2NO_2 + C \rightarrow CO_2 + 2NO \quad (2)$$

$$2NO_2 + 2C \rightarrow 2CO_2 + N_2 \quad (3)$$

Investigations on model soot oxidation revealed that NO_2 is a wider and stronger oxidant than O_2 at temperatures below 500 °C [49]. Additionally, the NO_x storage capacity was also considered as an essential factor for promoting soot combustion because the interplay between soot and nitrates. In the presence of stored nitrates, soot is oxidized through two routes [27]: oxidation with NO_2 and oxidation with O_2. Therefore, the stored nitrates can also help to lower the temperature of soot oxidation. In the temperature-programmed process, NO_2 can be generated from NO oxidation or decomposition of stored NO_x which oxidizes soot to CO_2 at lower temperature with itself reduced to NO or N_2. As shown in Fig. 7c, a maximum N_2 concentration of about 125 ppm was also detected in the TPO reactions together with traces of N_2O formation over C/LC sample. The formation curves for CO_2 and N_2 are similar in the same temperature range, evidencing the occurrence of simultaneous NO_x-soot reactions.

The promotion effect of NO_x on soot combustion is more obvious on C/LC with T_5 decreased to 288 °C while T_{50} decreased to 385 °C. The difference between T_{50} values in O_2 and $NO + O_2$ is defined as ΔT_{50} which can reflect the extent of NO_x effect on soot combustion. The larger ΔT_{50} on C/LC than LCC may be due to its higher NO_2 production capacity and NO_2 participation as an oxidizing agent. The participation of NO_2 in soot combustion was revealed in Fig. 8 which showed the NO_2 oxidation curves on catalysts with or without soot. In comparison with the Cs-doped sample, a larger amount production and consumption of NO_2 was both presented on C/LC. This can be ascribed to the promoted oxidation activity and subsequently make NO_2 catalyzed soot combustion efficiently. Most efficient soot oxidation is achieved in the case when there is a match between the nitrates decomposition and the temperature of soot oxidation by NO_2 [27]. According to the TPD profile, optimal interval for NO_x release should be at the temperature range from 300 to 450 °C in which most of soot particles was consumed as shown in Fig. 7b. The superior soot oxidation activity on C/LC under tight conditions was related to its higher NO_2 productivity, larger NO_2 consumption and more stored nitrates accessible in soot oxidation process.

The active NO_2 can reach the carbon surface more easily under loose contact conditions than that under tight conditions. Thus, the loose contact is also an appropriate way to investigate the effect of NO_x/O_2 compare to O_2 only. We have done the additional soot oxidation experiments under loose contact conditions. The activity parameters are summarized in Table 3. It can be seen from Table 3 that the activity enhancement after Cs introduced is more obvious under loose conditions in O_2, also revealing the promoting effect of Cs incorporation. Most importantly, in the presence of NO/O_2 atmosphere, the catalytic performance for soot oxidation under loose contacts decreases by the following order: LC > C/LC > LCC, which is consistent with NO_2 production capacity. This also indicates the promotion effect of NO_x on catalytic soot oxidation. The combustion of soot over the $LaCoO_3$ perovskite catalysts under loose contact conditions mainly occurs through NO_2-assisted mechanism. Besides, the promotion effect of Cs incorporation on soot oxidation in O_2 can be related to the low melting point of alkali metal Cs. It may give rise to highly mobile species on the soot surface which enhances the soot-catalyst contact, thus improving the catalytic activity.

Regarding NO_x variation under tight contact conditions, higher NO_x removal rate was observed after Cs introduced as shown in Table 2. It indicates that Cs ions are favorable to trapping the acidic NO_x due to stronger basicity. The introduction of cesium permit to reach the higher NO_x conversion, despite a lower NO_2 formation is evidenced in this case.

There are two factors that affect the solid–solid–gas reaction system of catalytic soot combustion. One is the intrinsic oxidation capability of the catalyst itself, which is related to the redox mechanism; the other is the contact condition between soot and catalyst, which is often associated with oxygen spillover [50]. Thus the enhanced activity of Cs-promoted samples on soot oxidation may be

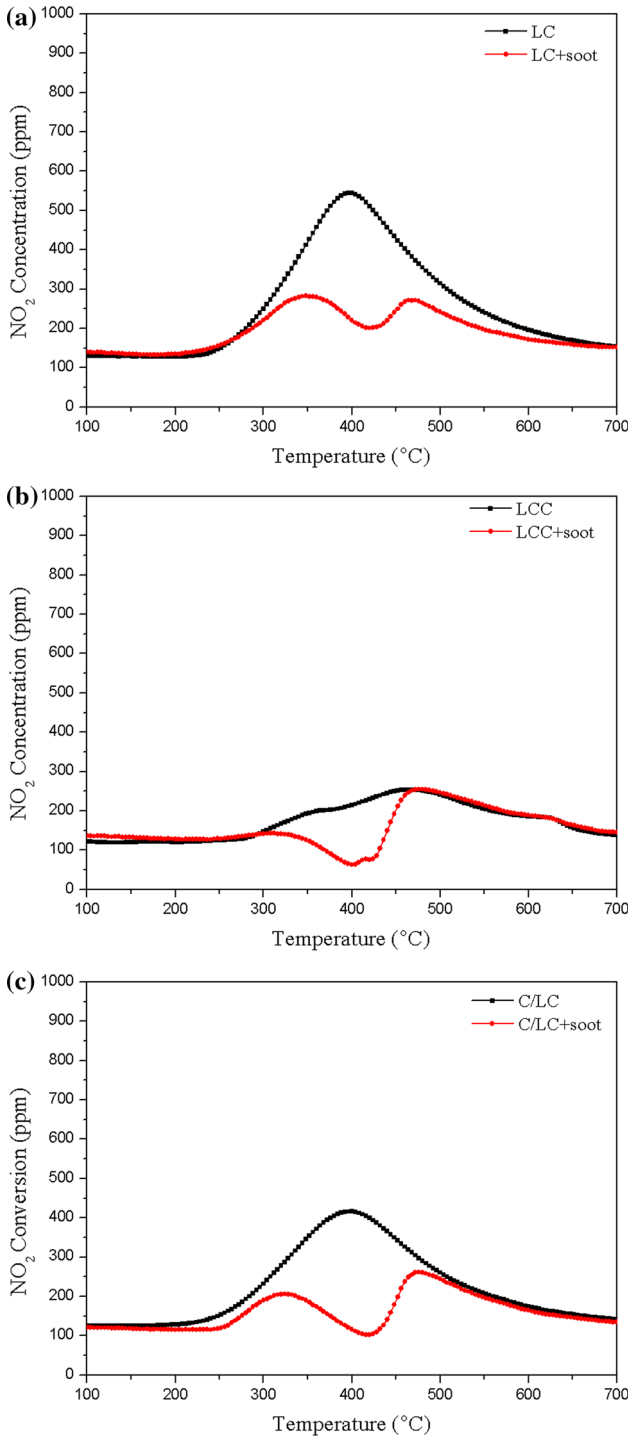

Fig. 8 NO_2 Concentration curves of on **a** LC, **b** LCC and **c** C/LC catalysts with or without soot

ascribed as follows: the improved contact condition between catalyst and soot, the promotion effect of NO_x adsorbed species, and the formation of more oxygen vacancies with increased oxygen mobility (for LCC)/enhanced oxidation of B-site cations (for C/LC).

Table 3 Catalytic performances for soot combustion under loose contact conditions

Samples	$C + O_2$		$NO + O_2$		ΔT_{50} (°C)
	T_5 (°C)	T_{50} (°C)	T_5 (°C)	T_{50} (°C)	
LC	428	492	314	417	75
LCC	395	469	359	434	35
C/LC	361	464	320	431	33

4 Conclusions

$LaCoO_3$ based perovskites with cesium introduction were successfully achieved for catalytic soot combustion. The different ways to introduce cesium have different impacts on the properties and activities of these catalysts. For Cs-supported sample, a promoted reduction of Co^{3+} to Co^{2+} ions was revealed, resulting in higher NO oxidation activity than that on Cs-doped sample. NO_x storage capacity was enhanced after Cs introduction due to the improved basicity. Cesium incorporation into $LaCoO_3$ decreased the ignition temperature in soot combustion under O_2 atmospheres which can be related to the enhanced oxygen mobility and the improved contact between soot and catalysts. In the presence of NO_x, Cs-supported catalyst exhibited higher soot oxidation activity than Cs-doped one, which was related to its higher NO_2 productivity, larger NO_2 consumption and more stored nitrates accessible in soot oxidation process. To sum up, the introduction of cesium hinders the NO-NO_2 conversion and favours nitrate surface species able to react with soot, yet it enhanced synergetic effects towards simultaneous abatement of soot and NO_x.

Acknowledgments This work is financially supported by the National Natural Science Foundation of China (Nos. 21007019 and 21277059), Shandong provincial key research Project (Nos. 2014GSF117039 and 2015GSF117025) and Shandong provincial natural science foundation, China (Nos. 2014ZRB01268 and ZR2015BL021).

References

1. Fino D, Bensaid S, Piumetti M, Russo N (2016) Appl Catal A 509:75–96
2. Neeft JPA, Makkee M, Moulijn JA (1996) Fuel Process Technol 47:1–69
3. Bueno-López A (2014) Appl Catal B 146:1–11
4. Monks PS, Granier C, Fuzzi S (2009) Atmos Environ 43:5268–5350
5. Roy S, Hegde MS, Madras G (2009) Appl Energy 86:2283–2297
6. Fino D (2007) Sci Technol Adv Mater 8:93–100
7. Zou G, Chen M, Shangguan W (2014) Catal Commun 51:68–71
8. van Setten BAAL, Makkee M, Moulijn JA (2001) Catal Rev 43:489–564

9. Jablonska M, Palkovits R (2015) Catal Sci Technol 6:49–72
10. Parks JE 2nd (2010) Science 327:1584–1585
11. Wang Z, Lu P, Zhang X, Wang L, Li Q, Zhang Z (2015) RSC Adv 5:52743–52753
12. Milt VG, Banús ED, Ulla MA, Miró EE (2008) Catal Today 133–135:435–440
13. Oi-Uchisawa J, Obuchi A, Wang S, Nanba T, Ohi A (2003) Appl Catal B 43:117–129
14. Liang Q, Wu X, Weng D, Xu H (2008) Catal Today 139:113–118
15. Wang K, Ping Z, Zhu JJ (2009) Catal Lett 131:672–675
16. Teraoka Y, Nakano K, Shangguan W, Kagawa S (1996) Catal Today 27:107–113
17. Fino D, Russo N, Saracco G, Specchia V (2006) J Catal 242:38–47
18. Jiménez R, García X, López T, Gordon AL (2008) Fuel Process Technol 89:1160–1168
19. Aneggi E, Leitenburg CD, Dolcetti G, Trovarelli A (2008) Catal Today 136:3–10
20. Mishra A, Prasad R (2014) Catal Rev 56:57–81
21. Wang H, Zhao Z, Liang P, Xu C, Duan A, Jiang G, Xu J, Liu J (2008) Catal Lett 124:91–99
22. Zhang G, Zhao Z, Liu J, Xu J, Jing Y, Duan A, Jiang G (2009) J Rare Earths 27:955–960
23. Liu J, Zhao Z, Xu C-m, Duan A (2008) Appl Catal B 78:61–72
24. Jelles SJ, van Setten BAAL, Makkee M, Moulijn JA (1999) Appl Catal B 21:35–49
25. Pushkin AN, Gulish OK, Koshcheeva DA, Shebanov MS (2013) Rus J Phys Chem A 87:23–27
26. Matarrese R, Castoldi L, Lietti L, Forzatti P (2008) Catal Today 136:11–17
27. Kustov AL, Makkee M (2009) Appl Catal B 88:263–271
28. Hong SS, Lee GD (2000) Catal Today 63:397–404
29. Legutko P, Kaspera W, Stelmachowski P, Sojka Z, Kotarba A (2014) Catal Commun 56:139–142
30. Fang S, Wang L, Sun Z, Feng N, Shen C, Lin P, Wan H, Guan G (2014) Catal Commun 49:15–19
31. Teraoka Y, Kanada K, Kagawa S (2001) Appl Catal B 34:73–78
32. Anandha Babu G, Ravi G, Hayakawa Y, Kumaresavanji M (2015) J Magn Magn Mater 375:184–193
33. Yu J, Jiang Z, Zhu L, Hao Z, Xu Z (2006) J Phys Chem B 110:4291–4300
34. Li Z, Meng M, Zha Y, Dai F, Hu T, Xie Y, Zhang J (2012) Appl Catal B 121–122:65–74
35. Wang Z, Jiang Z, Shangguan W (2007) Catal Commun 8:1659–1664
36. Makshina EV, Sirotin SV, Yushchenko VV, Mazo GN, van den Berg MWE, Klements'ev KV, Grünert W, Romanovskii BV (2006) Kinet Catal 47:49–53
37. Engelmann-Pirez M, Granger P, Leclercq G (2005) Catal Today 107–108:315–322
38. Sun M, Wang L, Feng B, Zhang Z, Lu G, Guo Y (2011) Catal Today 175:100–105
39. Kim CH, Qi G, Dahlberg K, Li W (2010) Science 327:1624–1627
40. Atribak I, Azambre B, Bueno López A, García-García A (2009) Appl Catal B 92:126–137
41. Aissat A, Siffert S, Courcot D (2012) Catal Today 191:90–95
42. Wang Z, Yan X, Bi X, Wang L, Zhang Z, Jiang Z, Xiao T, Umar A, Wang Q (2014) Mater Res Bull 51:119–127
43. Liu Z, Woo SI (2006) Catal Rev 48:43–89
44. Nova I, Castoldi L, Lietti L, Tronconi E (2004) J Catal 222:377–388
45. Prinetto F, Ghiotti G, Nova I, Lietti L, Tronconi E, Forzatti P (2001) J Phys Chem B 105:12732–12745
46. Mahzoul H, Brilhac JF, Gilot P (1999) Appl Catal B 20:47–55
47. Zhong Z, Chen K, Ji Y, Yan Q (1997) Appl Catal A 156:29–41
48. Yang Q, Gu F, Tang Y, Zhang H, Liu Q, Zhong Z, Su F (2015) RSC Adv 5:26815–26822
49. Wang Z, Zhang X, Wang L, Zhang Z, Jiang Z, Xiao T, Umar A, Wang Q (2013) Sci Adv Mater 5:1449–1457
50. Zhang Z, Zhang Y, Wang Z, Gao X (2010) J Catal 271:12–21